

Journal of Science and Transport Technology

Journal homepage: https://jstt.vn/index.php/en



Article info Type of article:

Original research paper

DOI:

https://doi.org/10.58845/jstt.utt.2 025.en.5.3.145-160

*Corresponding author:

Email address: quyendm@utt.edu.vn

Received: 06/05/2025
Received in Revised Form:

11/09/2025

Accepted: 22/09/2025

Vibration analysis of a mobile military repair vehicle during movement

Quyen Dao Manh^{1*}, Thang Tran Duc²

¹Country Institute of Mechanical Engineering, University of Transport Technology, 54 Trieu Khuc, Thanh Xuan, Hanoi, Vietnam, 11400 ²Institute of Vehicle and Energy Engineering, Le Quy Don Technical University, 236 Hoang Quoc Viet, Hanoi, Vietnam, 11900

Abstract: Military mobile repair vehicles are specialized vehicles capable of lifting, holding, and moving loads on complex terrain. The article presents a dynamic model of military mobile repair vehicles when holding and moving loads on road surfaces with random or harmonic profiles. The dynamic model considers the elastic deformation of tires, suspension systems, hoisting cables, and wind resistance acting on the loads during vehicle movement. This is a unique dynamic model due to the combination of crane and three-axle truck models. Lagrangian equations are applied to establish a system of differential equations describing the oscillations of the system and solve them using simulation methods in Matlab software. The results of the article indicate the displacements, velocities, and accelerations of all components in the system, particularly demonstrating the oscillation of the load when the vehicle moves on road surfaces with different profiles and velocities. The results of the article provide a basis for evaluating the process of holding and moving loads by military mobile repair vehicles across various terrains. The recommendation is to hold and move loads at a slow speed ranging from 2 m/s to 3 m/s. The findings also serve as input for proposing stable control solutions for the base vehicle and the load during movement.

Keywords: Mobile repair vehicle; Dynamic; Road surface; Random profile; Three-axle truck.

1. Introduction

Military mobile repair vehicles play a crucial role in maintaining and enhancing the combat capability of military forces by providing repair and maintenance capabilities on the battlefield. These mobile repair vehicles are designed to tow and repair damaged or stranded combat vehicles on the battlefield. They often can lift, tow, and transport heavy vehicles, even in difficult terrain conditions. They are primarily used to repair and maintain military vehicles such as tanks, armored vehicles, and wheeled vehicles on the battlefield.

Mobile repair vehicles based on the Zil 131 chassis, produced by Russia, can be used in many countries around the world, especially in countries that have military or commercial partnerships with Russia or have military forces using Soviet or Russian military equipment, such as Belarus, Kazakhstan, Kyrgyzstan, Armenia, Tajikistan, and Vietnam. Currently, in Vietnam, mobile repair vehicles such as the MRIV and MTO-AT based on the Zil 131 chassis produced by the Soviet Union are being used (Fig. 1) [1].

A common occurrence during the use of

military mobile repair vehicles is lifting and relocating loads to different locations. For example, lifting an engine from a damaged armored vehicle and transporting it to a nearby repair site. When comparing the working characteristics of the MTO-AT or MRIV mobile repair vehicles in lifting and moving loads with the processes involved in using wheel cranes, crawler cranes, or trucks for transportation, we can observe several distinctive features:

- i) While conventional trucks only provide transportation, military mobile repair vehicles not only lift and hold loads but also move on the road.
- ii) Wheel cranes or crawler cranes typically lift and hold loads in place, whereas the base vehicle remains stationary, contrasting with the mobility of the base vehicle of a mobile military repair vehicle.
- iii) Military mobile repair vehicles like the MTO-AT can lift and move loads across various terrains, particularly in complex terrains such as mountainous regions.

It can be observed that the dynamic modeling of military mobile repair vehicles when holding and moving loads is a combination of two fundamental research models: the dynamic model of truck motion and the dynamic model of crawler crane or wheel crane operation for stationary lifting. There have been numerous publications on the dynamics of wheel cranes, crawler cranes, or multi-axle truck dynamics.

The elastic deformation of cables is considered akin to a damping-spring system, as described by many authors in research papers on the dynamics of wheel cranes [2] [3], crawler cranes [4] [5] [6] [7], tower cranes [8] [9] [10] [11], gantry cranes [12] [13] [14], or ship-mounted cranes [15]. The total deformation of the cable is composed of static and dynamic deformations. Here, our focus lies on the lifting and hoisting cables. Thus, the correlation in research models is most evident in the context of crawler cranes. Studies also mention the effects of wind loads on the lifted load, which are detailed in various

documents [16] [17] [18]. The oscillation research of two-axle trucks is presented in documents [19] [20] [21] [22], while studies on the oscillation of three-axle or multi-axle trucks are detailed in documents [23] [24] [25] [26]. Research on truck oscillations during motion typically considers tire elasticity, suspension systems, and the influence of road surface deformation. Notably, authors often focus on two main issues:

- i) The first issue is the research on the role and influence of the suspension system structure on the oscillation process of the vehicle while it moves on the road. This aims to propose control strategies to enhance the smoothness of the vehicle's motion.
- ii) The second issue is the influence of road surface deformation on the vehicle's motion process. Specifically, examining the oscillation of the vehicle body, its axles, and loads attached to the vehicle body.

For road surface profiles, they are commonly categorized into three types: step profiles, harmonic profiles, and random profiles. Step or harmonic road surface profiles can be described by time-dependent functions. simple However. surface profiles pose challenges. Random road surface profiles are defined according to ISO 8608 standards, and there have been publications describing random road surface profiles in the time domain using Matlab simulation software [27] [28] [29].

Currently, countries are conducting research and development of mobile repair vehicles by applying advanced technologies and modern design methods to improve their performance, reliability, and flexibility. Some key trends in the development of mobile repair vehicles include the integration of information and communication technologies; the use of high-quality materials and structures; the implementation of automation technology; the integration of new engine and energy technologies; and the enhancement of vehicle safety and security. Countries with advantages in researching and manufacturing

mobile repair vehicles are typically those with developed industries, strong technical resources, research development and leading and organizations. Countries such as the United States, Russia, China, Germany, France, and the United Kingdom often heavily invest in research and development, possess high-quality technical infrastructure, and have skilled technical personnel, thereby giving them an edge in researching and manufacturing various types of mobile repair vehicles for military purposes. In some economically challenged countries, the MTO-AT mobile repair vehicle is still being utilized. However. there is a pressing need

improvements to enhance its effectiveness. This need for improvements is highly prioritized and closely monitored by many countries.

The article presents the results of a dynamic study of mobile repair vehicles during lifting and transportation processes. This is a theoretical study but holds significant practical implications, especially in the field of national security and defense. The research findings serve as a basis for evaluating the process of lifting and transporting loads across various terrains. Additionally, they can be utilized to improve mechanical assemblies and drive systems for equipment on board these vehicles.



Fig. 1. The mobile repair vehicles MTO-AT [1]

2. Methods and material

2.1. System description

The dynamic modeling of mobile repair vehicles during load holding and movement is established with the following assumptions: The vehicle moves uniformly on a straight and horizontal path; neglecting lateral oscillations of the vehicle and ground slope; the road surface profile is either harmonic or random, and the load is subjected to wind load $F_{\rm w}$ acting opposite to the direction of vehicle motion (Fig. 2).

The lifting boom is connected to the base vehicle via a hinge joint and held by a cable attached to the vehicle body, neglect friction in the rotary joints. The base vehicle is a three-axle truck with a balanced, dependent rear axle. During vehicle motion, the hoisting cable holding the load

is assumed to be non-extendable and always taut, while the load oscillates along the longitudinal plane of the base vehicle around its equilibrium position.

The entire system is placed in a fixed coordinate system Oxz attached to the ground. The masses are considered to be absolutely rigid. Let G_i ($i = 1 \div 6$) be the center of mass positions of the respective masses m_i . The generalized coordinate vector to investigate the system are:

$$q = [q_1 \quad q_2 \quad q_3 \quad q_4 \quad q_5 \quad q_6 \quad q_7]^{1}$$
 (1)

Where: q_1 (m) is the vertical displacement of the front axle, q_2 (m) is the vertical displacement of the middle axle, q_3 (m) is the vertical displacement of the rear axle, q_4 (m) is the vertical displacement of

the vehicle body, q_5 (rad) is the pitch angle of the vehicle body, q_6 (rad) is the pitch angle of the lifting

boom, and \mathbf{q}_7 (rad) is the angle defining the position of the load.

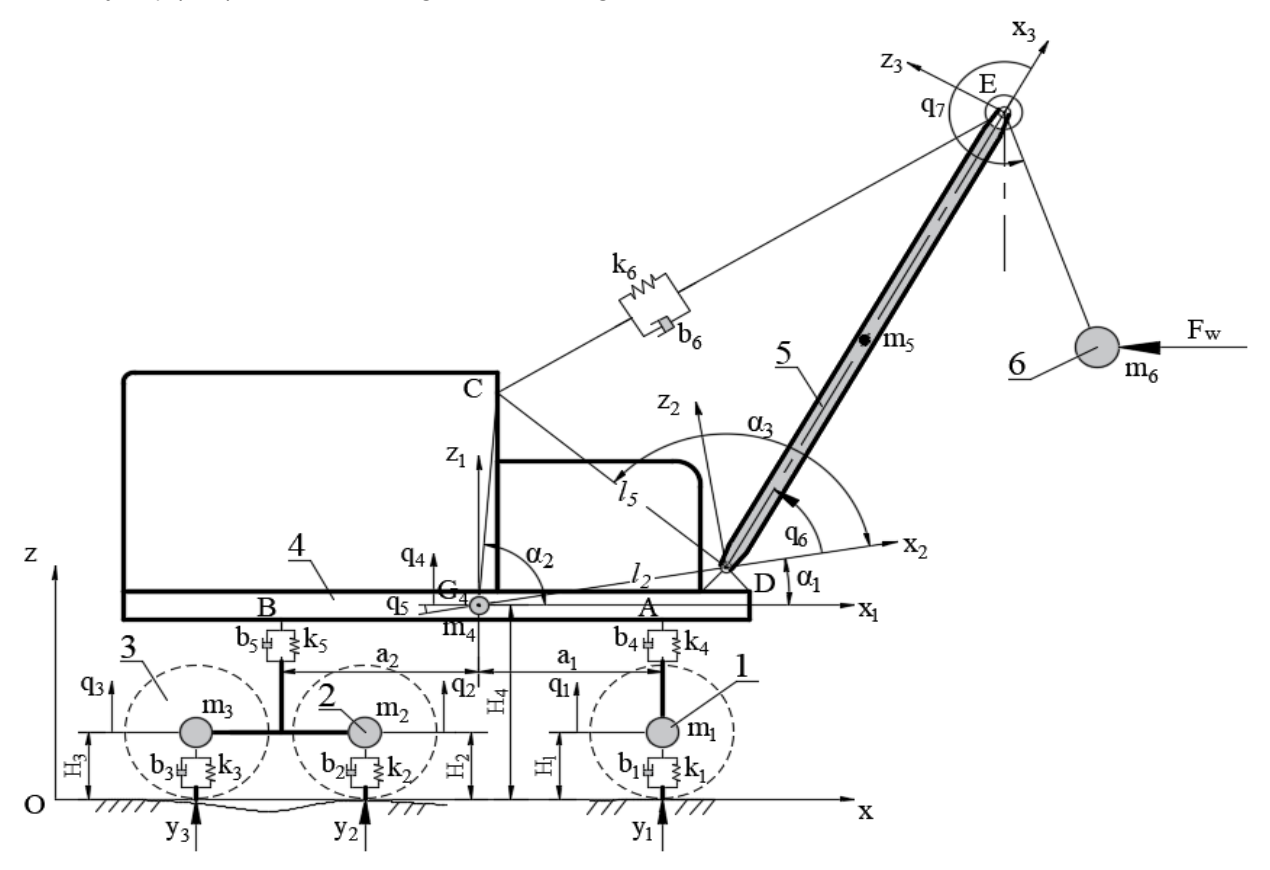


Fig. 2. The dynamic model of military mobile repair vehicle: 1- front axle, 2- middle axle, 3- rear axle, 4- base vehicle body, 5- boom, 6- load

Table 1. Table of Structural Parameters

Table 1. Table of Structural Farameters		
Parameters	Value	
Mass of the front axle m ₁ (kg)	305	
Mass of the middle axle m ₂ (kg)	60	
Mass of the rear axle m ₃ (kg)	60	
Mass of the base vehicle body m ₄ (kg)	6460	
Mass of the lifting boom m₅ (kg)	150	
Mass of the load m ₆ (kg)	500	
The stiffness coefficient k_1 (N/m) and the damping coefficient b_1 (N.s/m) of the front tires,	800000, 7800	
respectively		
The stiffness coefficient k_2 (N/m) and the damping coefficient b_2 (N.s/m) of the middle tires, respectively	800000, 7800	
The stiffness coefficient k_3 (N/m) and the damping coefficient b_3 (N.s/m) of the rear tires, respectively	800000, 7800	
The stiffness coefficient k4 (N/m) and the damping coefficient b4 (N.s/m) of the front suspension	195000,	
system, respectively	24000	
The stiffness coefficient k_5 (N/m) and the damping coefficient b_5 (N.s/m) of the rear suspension	295000,	
system, respectively	11500	
The stiffness coefficient k_6 (N/m) and the damping coefficient b_6 (N.s/m) of the boom holding cable, respectively	2000000, 500	
Inertial moments of the chassis (kg.m²)	8250	
Inertial moments of the boom (kg.m²)	320	

Table 2. Geometric dimensions

Parameters	Value
Length of segment CG ₄ , I ₁ (m)	1.95
Length of segment DG ₄ , I ₂ (m)	2.3
Length of segment DG ₅ , I ₃ (m)	2.5
Length of segment DE, I ₄ (m)	5
Length of segment CD, I₅ (m)	2.9
Length of segment EG $_6$, L $_0$ (m)	2
Initial positions of m ₁ , H ₁ (m)	0.65
Initial positions of m ₂ , H ₂ (m)	0.65
Initial positions of m ₃ , H ₃ (m)	0.65
Initial positions of m ₄ , H ₄ (m)	1.14
The horizontal distance AG ₄ , a ₁ (m)	2.1
The horizontal distance BG ₄ , a ₂ (m)	1.35
Distance between the axes of the front and middle axles, d1 (m)	2.725
Distance between the axes of the front and rear axles, d ₂ (m)	3.795
Angle $ extstyle extstyl$	0.174
Angle $\frac{\angle CGx_1}{\angle CG_4x_1}$, α_2 (rad)	1.535
Angle $\angle CDx_2$, α_3 (rad)	1.73

The dynamic parameters for studying the oscillations of the system are presented in Table 1. The geometric dimensions for studying the oscillations of the system are presented in Table 2.

2.2. The system of differential equations describing the oscillation of the system

2.2.1. The road surface profile

The height profile of the road surface changes over time. The profile of the road surface can be a random function, as presented in documents [27] [28] [29]. Additionally, the profile of the road surface can be considered a periodic function or a harmonic function. The road surface with random profile is determined according to ISO 8608 standards, depending on the speed of the vehicle during movement. If the length of road profile is L and the sampling interval is B, the maximum theoretical sampling spatial frequency is n_{max} = 1/B; x is the abscissa variable from 0 to L; $\Delta n = 1/L$; N = $n_{max}/\Delta n = L/B$; k is a constant value depending from ISO road profile classification, it assumes integers increasing from 3 to 9, corresponding to the profiles from class A to class H; $n_0 = 0.1$ cycles/m; ϕ random phase angle following an uniform probabilistic distribution within

the $0 \div 2\pi$ range. According to [28], the height of the road surface profile along the distance is determined by the expression (2)

If we consider the vehicle speed to be constant, then we have x = vt. Thus, the road surface profile class E, N = 2500, k = 7, corresponding to the vehicle's speed is depicted over the time domain corresponding to different speeds, as shown in Fig. 3.

Considering the road surface profile in the form of a sine wave graph, which is a very common type of road surface, the excitation function from the road surface acting on the vehicle chassis is as follows (3)

Where:
$$\omega = \frac{2\pi V}{S}$$
 with ω being the frequency

of the oscillation excitation; S is the wavelength of the road surface; d_1 is the distance between the axes of the front and middle axles; d_2 is the distance between the front and rear axles.

2.2.2. The kinetic energy of the system

The kinetic energy of the system includes the kinetic energy of the vehicle's axles, the kinetic energy of the vehicle body, the kinetic energy of the lifting boom, and the kinetic energy of the load.

Let v be the speed of the base vehicle, and set $q_{56}=q_5+q_6; q_{67}=q_6+q_7; q_{567}=q_5+q_6+q_7;$ $\dot{q}_{56}=\dot{q}_5+\dot{q}_6; \dot{q}_{67}=\dot{q}_6+\dot{q}_7; \dot{q}_{567}=\dot{q}_5+\dot{q}_6+\dot{q}_7.$

The expression defining the total kinetic energy of the system is (4)

2.2.3. The potential energy of the system

The total potential energy of the system is defined by the expression (5)

Where: ΔI is the total deformation of the boom holding cable CE; y_1 , y_2 and y_3 , respectively, represent the height of the road profile at the contact point between the wheels and the road surface.

Let q_{50} and q_{60} respectively denote the initial values of q_5 and q_6 . The length of segment CE at any given time is (6)

The static deformation of the cable segment *CE* at the initial time is determined from the static tension force through the equilibrium equation of moments of the forces acting on the lifting boom about point D. The static tension force in the cable is determined by the expression (7)

The static deformation of the cable segment CE is (8)

The total deformation of the cable segment CE is (9)

2.2.4. Dissipation energy function

The total dissipation energy of the system is

determined by the expression (10)

From Eq.3 and Eq.9, we have (11)

2.2.5. Vector of generalized force

Besides the influence of the road surface profile on the vehicle's motion, there is also wind resistance acting on the load and the wind resistance area of the vehicle's body. Due to the slow movement speed of the vehicle while holding and moving the load, the effect of wind resistance on the movement of the base vehicle is negligible. Let $A_w = 0.25 \text{ m}^2$ be the wind resistance area of the load, and $q_w = 250 \text{ N/m}^2$ be the wind resistance coefficient. Then, the wind resistance force F_w acting on the load is determined by the formula (12)

The vitual work done by the external force acting on the system is (13)

2.2.6. The system of differential equations

Applying the Lagrange equation of the second kind to write the system of differential equations describing the oscillation of the system in the form (14)

Then we obtain the system of differential equations describing the oscillation of the system as follows (15) (16) (17) (18) (19) (20) (21)

The system of differential equations (15-21) was solved using a simulation approach based on the Runge–Kutta algorithm and implemented in MATLAB software with the initial conditions is (22)

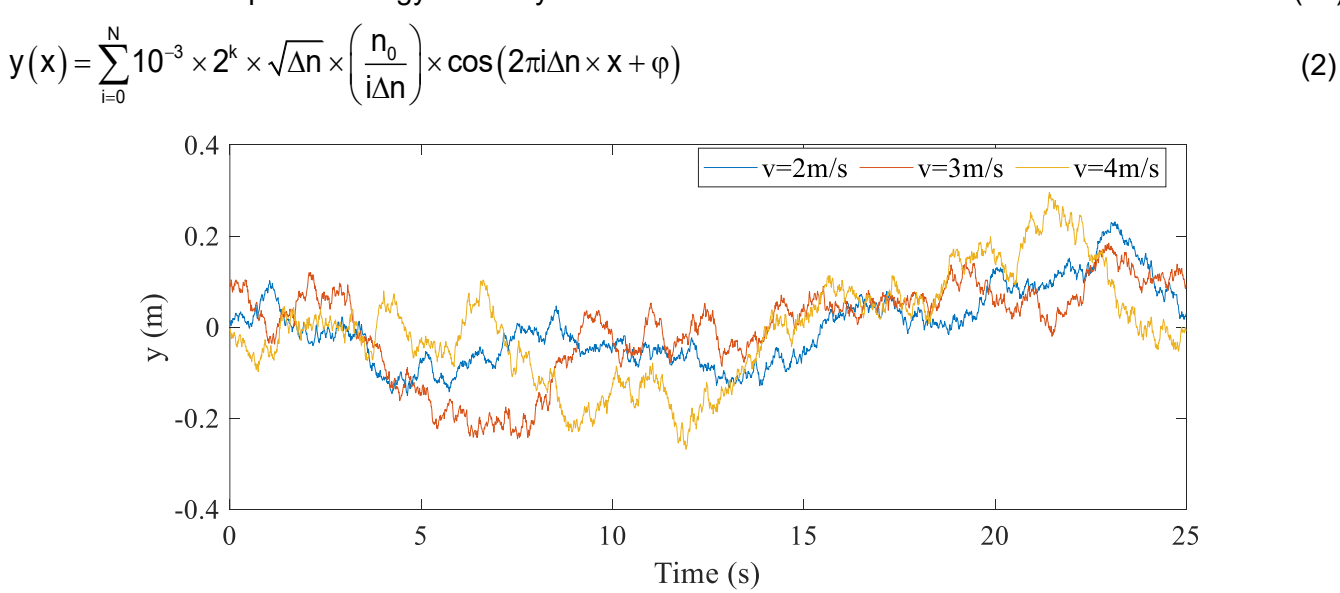


Fig. 3. Road surface profile class E corresponding to different speeds

$$y_1 = y_0 \sin \omega t; y_2 = y_0 \sin \left(\omega t - \frac{2\pi d_1}{S} \right); y_3 = y_0 \sin \left(\omega t - \frac{2\pi d_2}{S} \right)$$
 (3)

$$T = \frac{1}{2} m_{_{1}} \left(v^{_{2}} + \dot{q}_{_{1}}^{^{2}}\right) + \frac{1}{2} m_{_{2}} \left(v^{_{2}} + \dot{q}_{_{2}}^{^{2}}\right) + \frac{1}{2} m_{_{3}} \left(v^{_{2}} + \dot{q}_{_{3}}^{^{2}}\right) + \frac{1}{2} m_{_{4}} \left(v^{_{2}} + \dot{q}_{_{4}}^{^{2}}\right) + \frac{1}{2} J_{_{4}} \dot{q}_{_{5}}^{^{2}} + \frac{1}{2} J_{_{5}} \dot{q}_{_{6}}^{^{2}}$$

$$+\frac{1}{2}m_{5}\begin{cases} v^{2}+{I_{2}}^{2}\dot{q}_{5}^{2}+{I_{3}}^{2}\dot{q}_{56}^{2}+\dot{q}_{4}^{2}-2v{I_{2}}\dot{q}_{5}\sin\left(q_{5}+\alpha_{1}\right)-2v{I_{3}}\dot{q}_{56}\sin\left(q_{56}+\alpha_{1}\right)\\ +2{I_{2}}I_{3}\dot{q}_{5}\dot{q}_{56}\cos{q_{6}}+2\dot{q}_{4}I_{2}\dot{q}_{5}\cos\left(q_{5}+\alpha_{1}\right)+2\dot{q}_{4}I_{3}\dot{q}_{56}\cos\left(q_{56}+\alpha_{1}\right) \end{cases} \tag{4}$$

$$\left. + \frac{1}{2} m_6 \begin{cases} v^2 + \dot{q}_4^{\ 2} + {I_2}^2 \dot{q}_5^{\ 2} + {I_4}^2 \dot{q}_{56}^{\ 2} + {L_0}^2 \dot{q}_{567}^{\ 2} - 2 v {I_2} \dot{q}_5 \sin \left(q_5 + \alpha_1\right) - 2 v {I_4} \dot{q}_{56} \sin \left(q_{56} + \alpha_1\right) \\ - 2 v {L_0} \dot{q}_{567} \sin \left(q_{567} + \alpha_1\right) + 2 {I_2} {I_4} \dot{q}_5 \dot{q}_{56} \cos q_6 + 2 {I_2} {L_0} \dot{q}_{567} \dot{q}_5 \cos \left(q_6 + q_7\right) + 2 {I_4} {L_0} \dot{q}_{567} \dot{q}_{56} \cos \left(q_7\right) \\ + 2 \dot{q}_4 {I_2} \dot{q}_5 \cos \left(q_5 + \alpha_1\right) + 2 \dot{q}_4 {I_4} \dot{q}_{56} \cos \left(q_{56} + \alpha_1\right) + 2 \dot{q}_4 {L_0} \dot{q}_{567} \cos \left(q_{567} + \alpha_1\right) \end{cases} \right\}$$

$$\Pi = \frac{1}{2}k_{_{1}}{{\left({{\boldsymbol{q}}_{_{1}}} - {{\boldsymbol{y}}_{_{1}}} \right)}^{2}} + \frac{1}{2}k_{_{2}}{{\left({{\boldsymbol{q}}_{_{2}}} - {{\boldsymbol{y}}_{_{2}}} \right)}^{2}} + \frac{1}{2}k_{_{3}}{{\left({{\boldsymbol{q}}_{_{3}}} - {{\boldsymbol{y}}_{_{3}}} \right)}^{2}} + \frac{1}{2}k_{_{4}}{{\left({{\boldsymbol{q}}_{_{4}}} - {{\boldsymbol{a}}_{_{1}}}{{\boldsymbol{q}}_{_{5}}} - {{\boldsymbol{q}}_{_{1}}} \right)}^{2}} + \frac{1}{2}k_{_{6}}\Delta {{\boldsymbol{I}}^{2}}$$

$$+0.5k_{5}\left(q_{4}+a_{2}q_{5}-\frac{q_{2}+q_{3}}{2}\right)^{2}+m_{1}g\left(H_{1}+q_{1}\right)+m_{2}g\left(H_{2}+q_{2}\right)+m_{3}g\left(H_{3}+q_{3}\right)\tag{5}$$

$$+m_4g(H_4+q_4)+m_5g(H_4+q_4+I_2\sin(q_5+\alpha_1)+I_3\sin(q_5+q_6+\alpha_1))$$

$$+ m_6 g \big(H_4 + q_4 + I_2 \sin \big(q_5 + \alpha_1 \big) + I_4 \sin \big(q_{56} + \alpha_1 \big) + L_0 \sin \big(q_{567} + \alpha_1 \big) \big)$$

$$CE = \sqrt{I_5^2 + I_4^2 - 2I_5I_4 \cos(\alpha_3 - q_6)}$$
 (6)

$$F_{c} = \frac{m_{5}gI_{3}\cos\left(q_{50} + q_{60} + \alpha_{1}\right) + m_{6}gI_{4}\cos\left(q_{50} + q_{60} + \alpha_{1}\right)}{I_{5}I_{4}\sin\left(\alpha_{3} - q_{60}\right)}\sqrt{I_{5}^{2} + I_{4}^{2} - 2I_{5}I_{4}\cos\left(\alpha_{3} - q_{60}\right)}$$
(7)

$$\Delta I_{t} = \frac{F_{c}}{K_{6}} \tag{8}$$

$$\Delta I = \Delta I_t + \sqrt{I_5^2 + I_4^2 - 2I_5I_4\cos\left(\alpha_3 - q_6\right)} - \sqrt{I_5^2 + I_4^2 - 2I_5I_4\cos\left(\alpha_3 - q_{60}\right)} \tag{9}$$

$$\Phi = \frac{1}{2}b_{1}\left(\dot{q}_{1} - \dot{y}_{1}\right)^{2} + \frac{1}{2}b_{2}\left(\dot{q}_{2} - \dot{y}_{2}\right)^{2} + \frac{1}{2}b_{3}\left(\dot{q}_{3} - \dot{y}_{3}\right)^{2}$$

$$+\frac{1}{2}b_{4}\left(\dot{q}_{4}-a_{1}\dot{q}_{5}-\dot{q}_{1}\right)^{2}+\frac{1}{2}b_{5}\left(\dot{q}_{4}+a_{2}\dot{q}_{5}-\frac{\dot{q}_{2}+\dot{q}_{3}}{2}\right)^{2}+\frac{1}{2}b_{6}\dot{\Delta}I^{2} \tag{10}$$

$$\dot{\Delta}I = \frac{-I_5 I_4 \sin(\alpha_3 - q_6) \dot{q}_6}{\sqrt{I_5^2 + I_4^2 - 2I_5 I_4 \cos(\alpha_3 - q_6)}}$$
(11)

$$\dot{\boldsymbol{y}}_{1} = \boldsymbol{y}_{0} \boldsymbol{\omega} \cos \boldsymbol{\omega} t; \\ \dot{\boldsymbol{y}}_{2} = \boldsymbol{y}_{0} \boldsymbol{\omega} \cos \boldsymbol{\omega} \bigg(\boldsymbol{\omega} t - \frac{2\pi \boldsymbol{d}_{1}}{S} \bigg); \\ \dot{\boldsymbol{y}}_{3} = \boldsymbol{y}_{0} \boldsymbol{\omega} \cos \boldsymbol{\omega} \bigg(\boldsymbol{\omega} t - \frac{2\pi \boldsymbol{d}_{2}}{S} \bigg)$$

$$F_{w} = q_{w}A_{w} \tag{12}$$

$$\delta W = F_{w} \begin{pmatrix} I_{2} \sin(q_{5} + \alpha_{1}) \delta q_{5} + I_{4} \sin(q_{5} + q_{6} + \alpha_{1}) (\delta q_{5} + \delta q_{6}) \\ + L_{0} \sin(q_{5} + q_{6} + q_{7} + \alpha_{1}) (\delta q_{5} + \delta q_{6} + \delta q_{7}) \end{pmatrix}$$
(13)

$$\frac{d}{dt}\left(\frac{T}{\partial \dot{q}_{i}}\right) - \frac{\partial T}{\partial q_{i}} + \frac{\partial \Pi}{\partial \dot{q}_{i}} + \frac{\partial \Phi}{\partial \dot{q}_{i}} = Q_{i}; (i = 1 \div 7)$$
(14)

$$m_{1}\ddot{q}_{1} + (b_{1} + b_{4})\dot{q}_{1} - b_{4}\dot{q}_{4} + b_{4}a_{1}\dot{q}_{5} + (k_{1} + k_{4})q_{1} - k_{4}q_{4} + k_{4}a_{1}q_{5} + m_{4}g = k_{1}y_{1} + b_{1}\dot{y}_{1}$$
(15)

$$\begin{bmatrix} q_{10} & q_{20} & q_{30} & q_{40} & q_{50} & q_{60} & q_{70} \end{bmatrix}^{T} = \begin{bmatrix} 0 & 0 & 0 & 0 & \frac{\pi}{4} & \frac{215 \times \pi}{180} \end{bmatrix}^{T}$$

$$\begin{bmatrix} \dot{q}_{10} & \dot{q}_{20} & \dot{q}_{30} & \dot{q}_{40} & \dot{q}_{50} & \dot{q}_{60} & \dot{q}_{70} \end{bmatrix}^{T} = \begin{bmatrix} 0 & 0 & 0 & 0 & 0 & 0 \end{bmatrix}^{T}$$

$$(22)$$

3. Results and discussion

3.1. The influence of road surface profiles

Mobile repair vehicles that hold and move

load typically have very slow speeds. We proceed to investigate the influence of two types of road surface profiles in two scenarios.

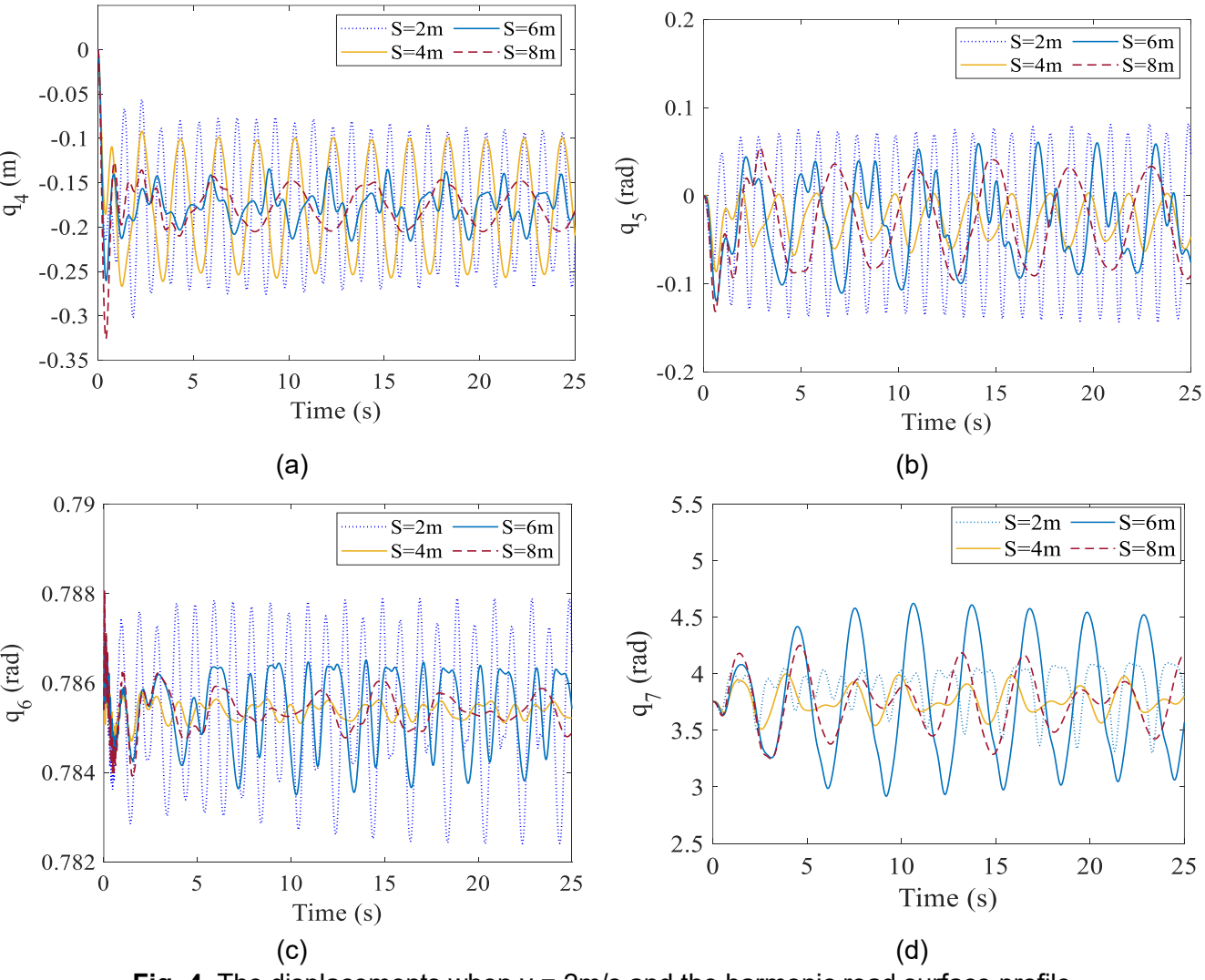


Fig. 4. The displacements when v = 2m/s and the harmonic road surface profile

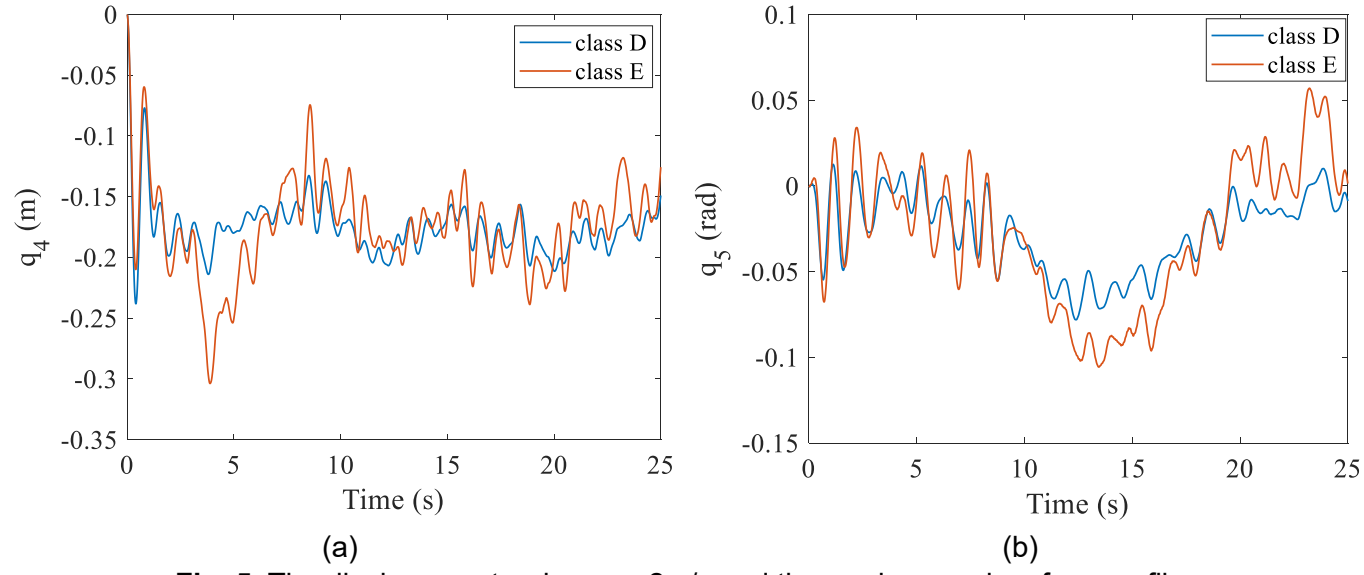


Fig. 5. The displacements when v = 2m/s and the random road surface profile

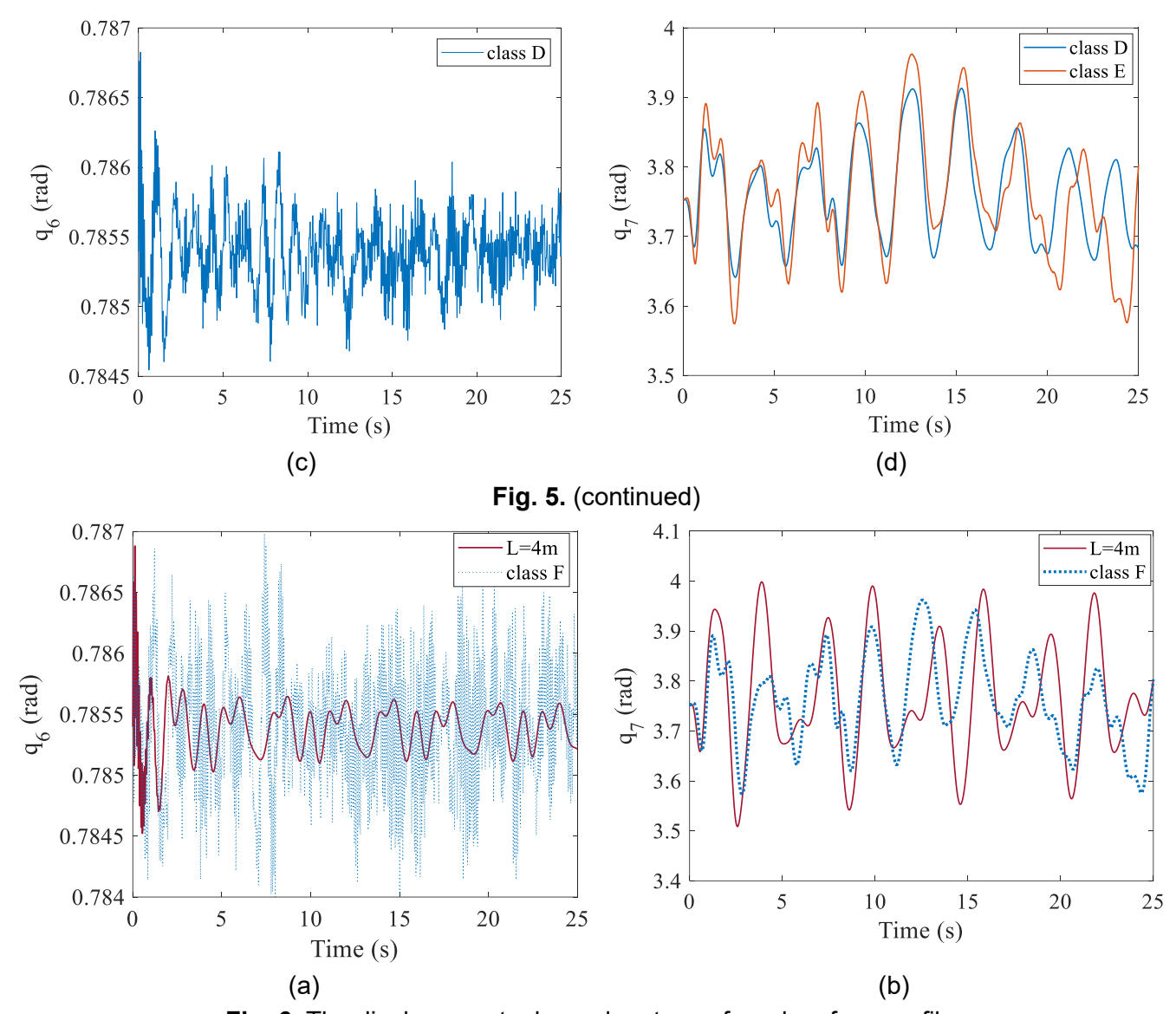


Fig. 6. The displacements depend on type of road surface profiles

In the first scenario, the vehicle moves on a road with a harmonic profile at a speed of 2 m/s, corresponding to a variation in the wavelength of the road surface from 2m to 8m. The results of the first investigation scenario are depicted in Fig. 4.

Fig. 4(a) illustrates the vertical displacement of the center of mass m_4 . The law of q_4 is harmonic, with the equilibrium position of q_4 corresponding to a value of about 17.5 cm. The oscillation amplitude of q_4 corresponds to wavelengths of 2 m, 4 m, 6 m, and 8 m, resulting in approximately 10 cm, 7.5 cm, 3.5 cm, and 2.5 cm, respectively. It is noteworthy that the oscillation amplitude along the vertical direction of the chassis is quite large when the wavelength is 2 m or 4 m. Thus, the larger the wavelength, the smaller the oscillation amplitude of

the center of mass m_4 . Meanwhile, the pitch angle q_5 of the chassis (Fig. 4(b)) also follows a similar pattern. For different wavelengths, the survey results show that the amplitude of the chassis pitch angle reaches its maximum value of about 0.066 rad for the 2m wavelength case and its minimum value of about 0.035 rad for the 4 m wavelength case. In contrast, the pitch angle of the chassis reaches its minimum value for this wavelength. Similarly, when the amplitude of q_4 is the smallest for the 8 m wavelength case, the pitch angle of the chassis is larger.

The oscillation of the load and the boom is a crucial issue. The graphs in Fig. 4(c) and Fig. 4(d) show that the laws of q_6 and q_7 also follow a harmonic pattern, varying according to the road

surface. Observing the graph in Fig. 4(c), we see that the pitch angle q_6 of the boom has a very small amplitude, with the maximum amplitude being only about 0.003 radians. From this, we can infer that as the vehicle moves, the weight of the load keeps the cable tensioned. During the vehicle's movement, the load swings back and forth around the equilibrium position.

In Fig. 4(d), we observe that the amplitude of q_7 reaches its maximum value for a 6 m wavelength and its minimum value for a 4 m wavelength, with intermediate values for 2 m and 8 m wavelengths. This indicates that the oscillation of the load is strongest when the vehicle moves on terrain with a harmonic road surface profile with a 6 m wavelength. In this case, the angle formed by the load suspension cable with the vertical line reaches its maximum value, approximately 0.79 radians, equivalent to 45°. When the wavelength is 4 m, the amplitude of q_7 is approximately 0.12 radians, corresponding to around 7°, indicating the most stable condition for the load.

In the second scenario, the vehicle moves at a speed of 2m/s on two types of road surfaces, labeled as class D and class E. The survey results are illustrated in Fig. 5.

Looking at the overall oscillation graphs of q_4 , q_5 , q_6 , and q_7 in Fig. 5, we can see that they also exhibit random variations, consistent with the stimulation from a random road surface profile. Although the variations do not follow a specific pattern when the vehicle moves on a randomly shaped road surface of classes D and E, the average values of q_4 , q_5 , q_6 , and q_7 over time are equivalent to their values in equilibrium when the vehicle moves on a harmonic road surface profile.

Examining the oscillation of components q_4 , q_5 , q_6 , and q_7 when the vehicle moves on road surfaces of classes D and E, we observe that, at the same speed of the vehicle, the chassis, boom, and load all oscillate more vigorously, with larger amplitudes on the class E road surface and smaller amplitudes on the class D road surface. This can also be inferred from the fact that the maximum

height of the irregularities on the class D random road surface is smaller than the maximum height of the irregularities on the class E road surface if the vehicle moves at the same speed. The influence of the irregular road surface is most evident in Fig. 5(c), where the oscillation angle of the boom oscillates with a high frequency around the initial value. Regarding the oscillation of the load, we observe that when moving on the class E road surface, the maximum oscillation angle of the load relative to the vertical is approximately 0.21 radians at a time of 12.5 seconds.

We continue to investigate the influence of a sinusoidal road surface with a wavelength of 4 m and a random road surface of class F when the vehicle moves at a speed of 2 m/s, in order to further clarify the effect of road type on the vibrations of the boom and the payload. Fig. 6 illustrates the influence of road surface types on the oscillation of the boom and the load. Fig. 6(a) indicates that the oscillation frequency of the boom is higher when the vehicle moves on the random road surface, while Fig. 6(b) shows that the oscillation amplitude of the load is greater when the vehicle moves on the harmonic road surface.

3.2. The influence of vehicle speed

In the first case, the vehicle moves on a harmonic road surface profile with a fixed wavelength of 5 m, corresponding to moving speeds ranging from 2 m/s to 6 m/s. The survey results are shown in Fig. 7.

The graphs in Fig. 7 all follow a common rule: as the velocity of the vehicle increases, the displacement of the chassis, the pitch angle of the chassis, the pitch angle of the boom, and the pitch angle of the load all increase in amplitude. The slower the vehicle moves, the smaller the amplitudes of the components q_4 , q_5 , q_6 , and q_7 . For the vertical oscillation q_4 of the vehicle body as shown in Fig. 7(a), the maximum amplitude is about 18 cm when v = 5 m/s, and the minimum is about 6 cm when v = 2 m/s. The pitch angle q_5 of the vehicle body in Fig. 7(b) has a very large amplitude of about 0.19 rad when the vehicle

moves fast with v = 5 m/s and a minimum amplitude of about 0.08 rad when v = 2 m/s. Fig. 7(c) shows the pitch angle of the boom, with a maximum amplitude of only about 0.005 rad, which is very small. More attention is paid to the pitch angle of the load. When v = 5 m/s, the amplitude of the payload q_7 is very large, up to 2.15 rad. When v =2 m/s, the amplitude of the payload q₇ is about 0.42 rad. During motion, the base vehicle, the boom, and the payload are subjected to combined influences from multiple factors, including structural characteristics and terrain-induced excitations. Consequently, the payload oscillates with a forced vibration frequency dependent on various complex factors. Between the 16th and 22nd seconds, the oscillation amplitude of the payload increases due to resonance

phenomenon, which may occur when the natural frequency of the payload and the combined frequency of the external forced excitations are very close. In the first 15 seconds, it is observed that at a speed of 4 m/s, the payload oscillation amplitude rises progressively and reaches higher values more quickly compared to the case at 3 m/s. Accordingly, this results in noticeable differences in the payload oscillation amplitudes during the last 10 seconds. The results presented here are theoretical, and in practice, it is not possible to simultaneously hold a load and move the vehicle at v = 5 m/s.

In the second case, the vehicle moves on a road surface with random profile of class E, with different moving speeds of 2 m/s, 3 m/s, and 4 m/s. The survey results are shown in Fig. 8.

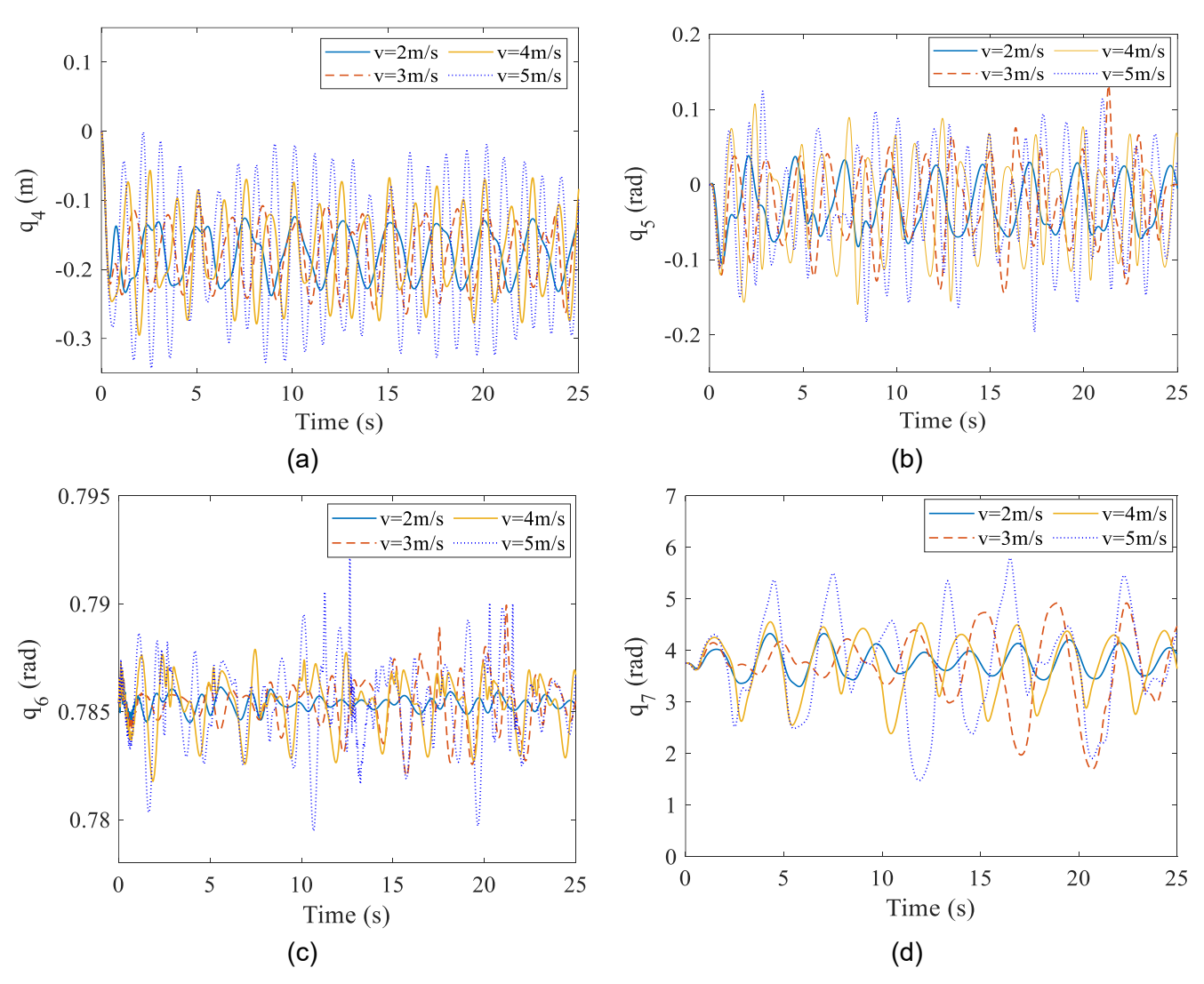


Fig. 7. The displacements when v varies and the harmonic road surface profile

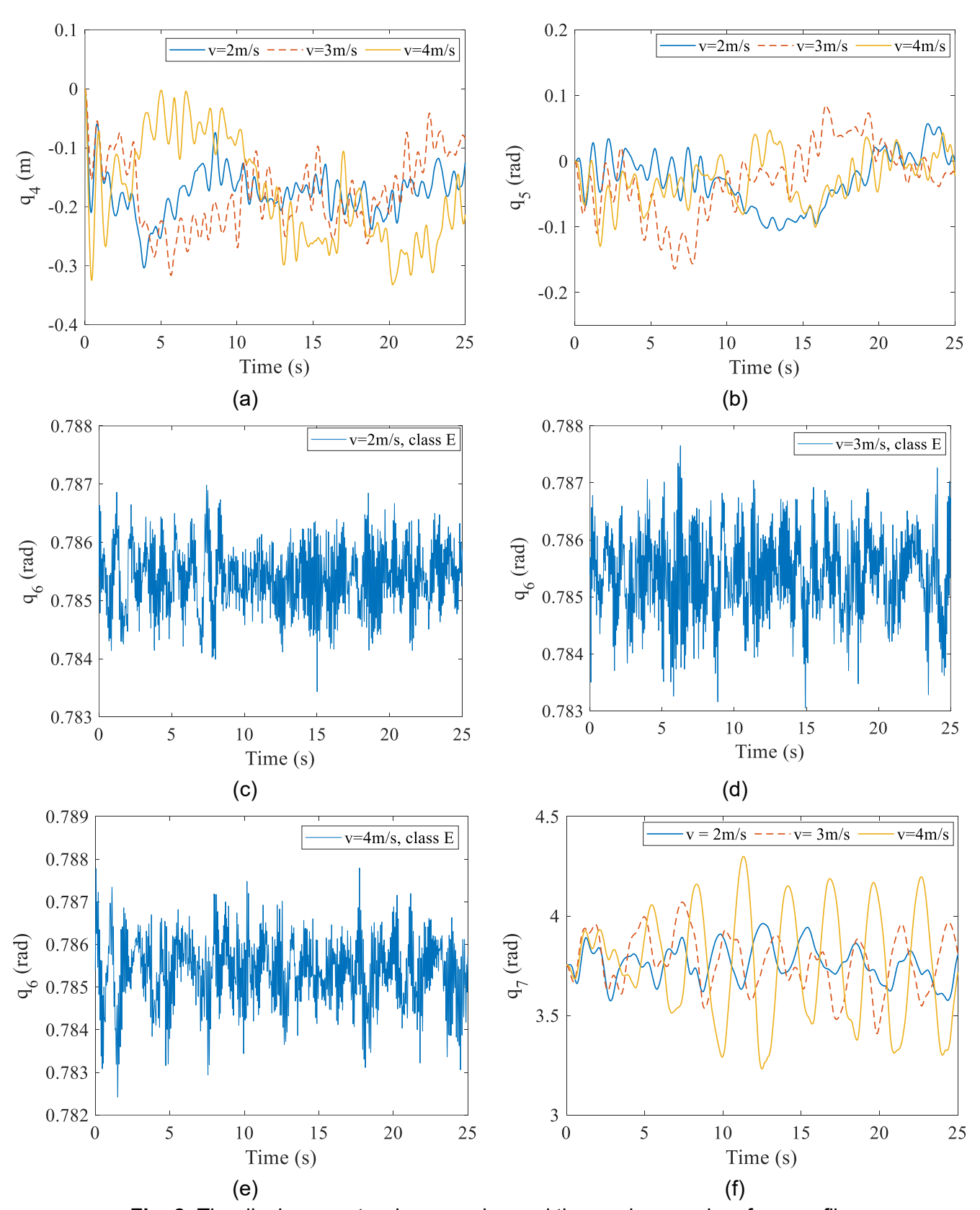


Fig. 8. The displacements when v varies and the random road surface profile

When the vehicle moves on a random road surface, the laws governing the components q_4 , q_5 , q_6 , and q_7 also vary randomly. However, they all have a common rule: the maximum amplitude

increases as the velocity of the vehicle increases. The results on the graphs in Fig. 8 also indicate that the vehicle should only be driven at a speed of 2 m/s because, at this speed, the load has the

smallest oscillation amplitude. In terms of payload vibration, the vehicle should not be operated at speeds of 4 m/s, since at this speed the oscillation amplitude of the payload increases by approximately 2.5 times compared to the cases of 2 m/s or 3 m/s.

The results presented in the above graphs are consistent with those reported in [30]. In that study, the Maintenance Armored Security Vehicle was examined under conditions of load retention and movement, using a two-axle wheeled armored vehicle as the base platform. These studies provide an important theoretical foundation for upgrading two-axle or three-axle military vehicles into mobile cranes when required to handle specific situations.

4. Conclusions

The laws depicted in the graphs are consistent with the stimuli from different types of road surfaces when the vehicle is in motion. However, this study only stopped at theoretical research and overlooked some factors related to the influence of slope and soil elasticity deformation when the vehicle moves, but it still achieved certain results. The key points of the paper's findings are as follows:

- i) A dynamic model of military mobile repair vehicles has been developed when both holding loads and moving on various types of road surfaces. This model is unique and distinct from crane models and models of trucks moving on roads.
- ii) The impact of different terrains and vehicle speeds on the oscillation of the vehicle body, boom, and load has been investigated. In particular, the vibration of the payload shows a very strong correlation with the vehicle speed under the same terrain conditions. At higher speeds of $4 \div 5$ m/s, the oscillation amplitude of the payload is more than twice that observed at speeds of $2 \div 3$ m/s.
- iii) Based on the results of this theoretical study, in terms of payload vibration, the vehicle should be operated at speeds ranging from 2 m/s to 3 m/s.

This research opens up a new direction for further research, which is to study the stable control options for loads when military mobile repair vehicles are both holding loads and moving on various terrains. Additionally, a 3D model of the load-holding and moving process of the vehicle could be constructed while comprehensively investigating the influence of slope and soil elasticity on the terrain.

References

- [1] Karopka. Modelers' forum (in Russia) https://karopka.ru/community/user/21500/?M ODEL=558846 (accessed 1 May 2025)
- [2] L.A. Tuan, L.V. Duong. (2022). Modeling and observer-based robust controllers for telescopic truck cranes. *Mechanism and Machine Theory*, 173. https://doi.org/10.1016/j.mechmachtheory.202 2.104869
- [3] R. Mijailović. (2011). Modelling the dynamic behaviour of the truck-crane. *Transport*, 26(4), 410-417.
 - https://doi.org/10.3846/16484142.2011.642946
- [4] S.-G. Lee, L.A. Tuan. (2017). Modeling and advanced sliding mode controls of crawler cranes considering wire rope elasticity and complicated operations. *Mechanical Systems* and *Signal Processing*, 103, 250-263. https://doi.org/10.1016/j.ymssp.2017.09.045
- [5] L.A. Tuan. (2019). Fractional-order fast terminal back-stepping sliding mode control of crawler cranes. *Mechanism and Machine Theory*, 137, 297-314.
 - https://doi.org/10.1016/j.mechmachtheory.201 9.03.027
- [6] K.-S. Hong, Q.H. Ngo. (2012). Adaptive sliding mode control of container cranes. *IET Control Theory & Applications*, 6(5), 662-668. https://doi.org/10.1049/iet-cta.2010.0764
- [7] S.-G. Lee, L. A. Tuan, N.L. Cong, et al. (2015). Robust controls for ship-mounted container cranes with viscoelastic foundation and flexible hoisting cable. *Proceedings of the Institution of Mechanical Engineers, Part I: Journal of*

- Systems and Control Engineering, 229(7), 662-674.
- https://doi.org/10.1177/0959651815573903
- [8] T-S. Wu, M. Karkoub, et al. (2016). Anti-sway tracking control of tower cranes with delayed uncertainty using arobust adaptive fuzzy control. *Fuzzy Sets and Systems*, 290, 118-137. https://doi.org/10.1016/j.fss.2015.01.010
- [9] H. Chen, Y. Fang, N. Sun. (2019). An adaptive tracking control method with swing suppression for 4-DOF tower crane systems. *Mechanical Systems and Signal Processing*, 123, 426-442. https://doi.org/10.1016/j.ymssp.2018.11.018
- [10] J. Vaughann, D. Kim, W. Singhose. (2010). Control of Tower Cranes With Double-Pendulum Payload Dynamics. *IEEE Transactions on Control Systems Technology*, 18(6), 1345-1358. https://doi.org/10.1109/TCST.2010.2040178
- [11] S.M. Fasih, Z. Mohamed, W. Anjum, et al. (2020). Payload swing control of a tower crane using a neural network–based input shaper. *Measurement and Control*, 53(7-8), 1171-1182. https://doi.org/10.1177/0020294020920895
- [12] R. Nishimoto, R. Kikuuwe. (2023). Position-Commanding Anti-Sway Controller for 2-D Overhead Cranes Under Velocity and Acceleration Constraints. *IEEE Access*, 11, 35069-35079.
- [13] W.J. Blajer, K.A. Kołodziejczyk. (2006). Trajectory planning and control of overhead cranes in the work environment with obstacles. *Modelowanie Inżynierskie*, 1(32), 53-60.
- [14] H. Liu, W. Cheng, Y. Li. (2019). Dynamic Responses of an Overhead Crane's Beam Subjected to a Moving Trolley with a Pendulum Payload. *Shock and Vibration*, 2019(6), 1-14. https://doi.org/10.1155/2019/1291652
- [15] X. Cao, C. Meng, Y. Zhou, et al. (2021). An improved negative zero vibration anti-swing control strategy for grab ship unloader based on elastic wire rope model. *Mechanics & Industry*, 22(45), 1-10. https://doi.org/10.1051/meca/2021045

- [16] D. Cekus, P. Kwiaton. (2020). Effect of the rope system deformation on the working cycle of the mobile crane during interaction of wind pressure. *Mechanism and Machine Theory*, 153, 104001. https://doi.org/10.1016/j.mechmachtheory.202 0.104011
- [17] H. Ouyang, X. Xu, G. Zhang, et al. (2021). Boom motion trajectory generation approach for load sway rejection in rotary cranes considering double-pendulum effect. *Measurement and Control*, 54(5-6), 924-934. https://doi.org/10.1177/0020294020944964
- [18] D. Cekus, P. Kwiaton, T. Geisler. (2021). The dynamic analysis of load motion during the interaction of wind pressure. Modelling and analysis of mechanical systems dynamics. *Meccanica*, 56, 785-796. https://doi.org/10.1007/s11012-020-01234-x
- J. Zhang, Y. Deng, N. Zhang, et al. (2019).
 Vibration Performance Analysis of a Mining Vehicle with Bounce and Pitch Tuned Hydraulically Interconnected Suspension.
 Chinese Journal of Mechanical Engineering, 32, 5.
 https://doi.org/10.1186/s10033-019-0315-0
- [20] T. Attia, K.G. Vamvoudakis, et al. (2019). Simultaneous dynamic system estimation and optimal control of vehicle active suspension. Vehicle System Dynamics, 57(10), 1467-1493. https://doi.org/10.1080/00423114.2018.152100 0
- [21] M. Boreiry, S.E.-Nejad, J. Marzbanrad. (2019). Sensitivity analysis of chaotic vibrations of a full vehicle model with magnetorheological damper. *Chaos, Solitons and Fractals*, 127, 428-442.
 - https://doi.org/10.1016/j.chaos.2019.07.005
- [22] A. Sezgin, Y.Z. Arslan. (2012). Analysis of the vertical vibration effects on ride comfort of vehicle driver. *Journal of Vibroengineering*, 14(2), 559-571.
- [23] T.D. Thang, D.V. Le, D.V. Chu. (2024). Research on the dynamics of a heavy

- mechanized bridge in the deployment phase of the lifting frame. *EUREKA: Physics and Engineering*, 1, 116-126. https://doi.org/10.21303/2461-4262.2024.003220
- [24] S. Basaran, M. Basaran. (2020). Vibration Control of Truck Cabins With the Adaptive Vectorial Backstepping Design of Electromagnetic Active Suspension System. *IEEE Access*, 8, 173056-173067. https://doi.org/10.1109/ACCESS.2020.302535
- [25] M. Demic, Z.B. Sakota, D.M. Miloradovic (2018). Impact of truck'spower trainlayout on driver's foreand-aft vibration loads. *Journal of Mechanical Engineering and Modern Technology*, 1(1), 37-51.
- [26] Y. Hu, V. Nguyen, Y. Ye. (2020). Vibration research of heavy trucks. Part 1: Sensitivity analysis of dynamic parameters on ride comfort. *Journal of Mechanical Engineering, Automation and Control Systems*, 1(2), 114-123.

https://doi.org/10.21595/jmeacs.2020.21813

- [27] M. Agostinacchio, D. Ciampa, S. Olita. (2014). The vibrations induced by surface irregularities in road pavements a Matlab® approach. *European Transport Research Review*, 6, 267-275 https://doi.org/10.1007/s12544-013-0127-8.
- [28] C.D. Jiang, L. Cheng, S. Fengchun, et al. (2012). Simulation of Road Roughness Based on Using IFFT Method. 2012 *Third World Congress on Software Engineering*, pp. 190-193. https://doi.org/10.1109/WCSE.2012.46
- [29] Y. Zhang, H.S. Zhao, S.T. Lie. (2018). A Simple Approach for Simulating the Road Surface Roughness Involved in Vehicle-Bridge Interaction Systems. *International Journal of Structural Stability and Dynamics*, 18(7), 1871009.
 - https://doi.org/10.1142/S0219455418710098
- [30]. Q.D. Manh, T.T. Duc, T.N. Huy, D.L. Van, D.C. Van. (2025). Research on Terrain Response of the Maintenance Armored Security Vehicle. *Gazi University Journal of Science*, 38(2), 959-971. https://doi.org/10.35378/gujs.1519763